

Article

Acrylate Copolymer-Reinforced Hydrogel Electrolyte for Strain Sensors and Flexible Supercapacitors

Ruixue Liu ¹, Wenkang Liu ¹ , Jichao Chen ¹, Xiangli Bian ^{2,*}, Kaiqi Fan ¹ , Junhong Zhao ¹ and Xiaojing Zhang ^{1,*}

¹ College of Materials and Chemical Engineering, Zhengzhou University of Light Industry, Zhengzhou 450002, China

² Puyang City Water Supply Co., Ltd., Puyang 457000, China

* Correspondence: maying01@zybank.com.cn (X.B.); zhangxj@iccas.ac.cn (X.Z.)

Abstract: Ionic conductive hydrogels with good conductivity and biocompatibility have become one of the research highlights in the field of wearable flexible sensors and supercapacitors. In this work, poly(methacrylic acid–methyl methacrylate)-reinforced poly(sodium acrylate–vinyl phosphonic acid) composite hydrogels (P(AAS-VPA)/PMMS) were designed and tested for strain sensor or supercapacitor applications. The results showed recoverability for 20 cycles of tension and compression experiments, an excellent breaking strain of 2079%, and ionic conductivity of $0.045 \text{ S}\cdot\text{cm}^{-1}$, demonstrating strong support for the application of the P(AAS-VPA)/PMMS hydrogel in strain sensors and supercapacitors. The composite hydrogel exhibited outstanding sensing and monitoring capability with high sensitivity ($\text{GF} = 4.0$). The supercapacitor based on the P(AAS-VPA)/PMMS composite hydrogel showed excellent capacitance performance (area capacitance $100.8 \text{ mF}\cdot\text{cm}^{-2}$ and energy density $8.96 \text{ }\mu\text{Wh}\cdot\text{cm}^{-2}$) at ambient temperature and even $-30 \text{ }^\circ\text{C}$ ($25.3 \text{ mF}\cdot\text{cm}^{-2}$ and $2.25 \text{ }\mu\text{Wh}\cdot\text{cm}^{-2}$). The hydrogel has stable electrochemical stability (1000 cycles, Coulomb efficiency $> 97\%$) and exhibits electrochemical properties similar to those in the normal state under different deformations. The excellent results demonstrate the great potential of the P(AAS-VPA)/PMMS composite hydrogel in the field of strain sensors and flexible supercapacitors.

Keywords: supercapacitors; latex particles; sensitivity; capacitance performance



Citation: Liu, R.; Liu, W.; Chen, J.; Bian, X.; Fan, K.; Zhao, J.; Zhang, X. Acrylate Copolymer-Reinforced Hydrogel Electrolyte for Strain Sensors and Flexible Supercapacitors. *Batteries* **2023**, *9*, 304. <https://doi.org/10.3390/batteries9060304>

Academic Editors: Yuanhua Xiao, Ling Wu, Xianwen Wu, Yiping Tang and Sang Bok Lee

Received: 17 March 2023

Revised: 26 April 2023

Accepted: 30 May 2023

Published: 31 May 2023



Copyright: © 2023 by the authors. Licensee MDPI, Basel, Switzerland. This article is an open access article distributed under the terms and conditions of the Creative Commons Attribution (CC BY) license (<https://creativecommons.org/licenses/by/4.0/>).

1. Introduction

With the development of science and technology, people are increasingly pursuing convenient lifestyles, which has led to an increasing emphasis on flexible electronic devices [1–3]. To create truly lightweight flexible electronic devices, the importance of two of these devices, wearable sensors [4,5] and flexible energy storage devices [6–8], cannot be overemphasized. The supercapacitor as an energy storage device has the benefits of fast charging and discharging rate, long-term service life, and high-power density compared with traditional batteries [9,10], which indicates that the application of the supercapacitor in supplying energy to flexible electronic devices has great potential. Strain sensors need to respond to externally applied deformation through changes in their resistance or capacitance [11,12]. As a result, strain sensors are required to have high sensitivity, high tensile strength, stability, and fast response speed; these features now form the mainstream direction of strain sensor design [13]. In contrast, conventional strain sensors have a maximum tensile strain of up to 5% and a GF value of up to 2 [14]. Obviously, these properties are no longer sufficient to meet people's needs. Liu et al. [15] reported a stretchable strain sensor based on carbon nanotubes (CNT)/silver nanowires (AgNW) capable of reaching a GF value of 6.7 with good durability (>1000 tensile cycles) and good response and recovery speeds (420 ms and 600 ms, respectively) for the measurement of finger movements. Moreover, PENG et al. [16] reported a novel multi-walled carbon nanotube (MWCNT)/ordered mesoporous carbon (OMC) composite fiber, which has the advantages of being lightweight

and features of conductivity and flexibility. The authors' team twisted two composite fibers to produce a wire-like double-layer capacitor with a specific capacitance of $39.7 \text{ mF}\cdot\text{cm}^{-2}$, an energy density of $1.77 \text{ }\mu\text{Wh}\cdot\text{cm}^{-2}$, and a maximum power density of $0.43 \text{ }\mu\text{W}\cdot\text{cm}^{-2}$. The above-mentioned materials used in sensors and supercapacitors are poorly stretched and do not adhere well to the surface of the material; therefore, the above-mentioned problems must be solved to achieve the manufacture of truly flexible electronic devices.

Hydrogels have good stretchability, adjustable hydrogel strength, and flexibility, which can be used to improve the flexibility of sensors and energy storage devices, and can be designed to obtain other excellent properties. Therefore, there is an urgent need to investigate hydrogel electrolytes with better flexibility. Zhu et al. [17] reported a hydrogel-based electronic skin composed of polyvinyl alcohol, citric acid, and silver nanoparticles, which has good tensile properties (596% strain) and a strain sensitivity of $\text{GF} = 1.6$ (0–200% strain), and it can monitor various human movements well. Jiang et al. [18] reported a hydrogel electrolyte prepared by introducing 2-acrylamido-2-methylpropanesulfonic acid (AMPS) monomer and Gly into a polyvinyl alcohol/polyacrylamide (PVA/PAM) double network hydrogel. This hydrogel electrolyte has a conductivity of up to $3.85 \text{ S}\cdot\text{m}^{-1}$. The authors' team prepared a hydrogel-based supercapacitor by coating carbon nanotube dispersions on the surface of the hydrogel electrolyte, which has a high specific capacity of $85.25 \text{ mF}\cdot\text{cm}^{-2}$ at a current density of $0.5 \text{ mA}\cdot\text{cm}^{-2}$.

In this study, to expand the application of flexible hydrogel electrolytes in the field of sensors and supercapacitors, poly (methacrylic acid–methyl methacrylate) [19] (referred to as PMMS) inter-entangled copolymer clusters as the physically crosslinked network were introduced into a chemically cross-linked poly (sodium acrylate–vinyl phosphonic acid) (P(AAS-VPA)) copolymer network to reinforce the flexibility and adhesion performance of the polyelectrolyte. The addition of VPA as the comonomer aims to provide stronger adhesion and ion transport capacity. The P(AAS-VPA)/PMMS composite hydrogel demonstrated high sensitivity ($\text{GF} = 4.0$) and excellent sensing and monitoring abilities, allowing it to quickly monitor a variety of human movements. The supercapacitor with excellent electrochemical performance and low-temperature resistance ($-30 \text{ }^\circ\text{C}$) was prepared by binding of the polyaniline layer onto the hydrogel surface using the deposition–oxidation method. The advantages mentioned above greatly expand the scope of the application of poly (sodium acrylate)-based composite hydrogels in flexible sensors and supercapacitors. A supercapacitor with excellent electrochemical properties (at a current density of $0.2 \text{ mA}\cdot\text{cm}^{-2}$, area capacitance $100.8 \text{ mF}\cdot\text{cm}^{-2}$, and an energy density of $8.96 \text{ }\mu\text{Wh}\cdot\text{cm}^{-2}$) and low-temperature resistance ($-30 \text{ }^\circ\text{C}$, $25.3 \text{ mF}\cdot\text{cm}^{-2}$ and $2.25 \text{ }\mu\text{Wh}\cdot\text{cm}^{-2}$) was prepared by combining a polyaniline layer onto the hydrogel surface using the deposition–oxidation method. The gel has stable electrochemical stability (1000 cycles, Coulomb efficiency $> 97\%$) and exhibits electrochemical properties similar to those in the normal state under different deformations. The above advantages greatly extend the scope of the application of poly (sodium acrylate)-based composite hydrogels in flexible sensors and supercapacitors.

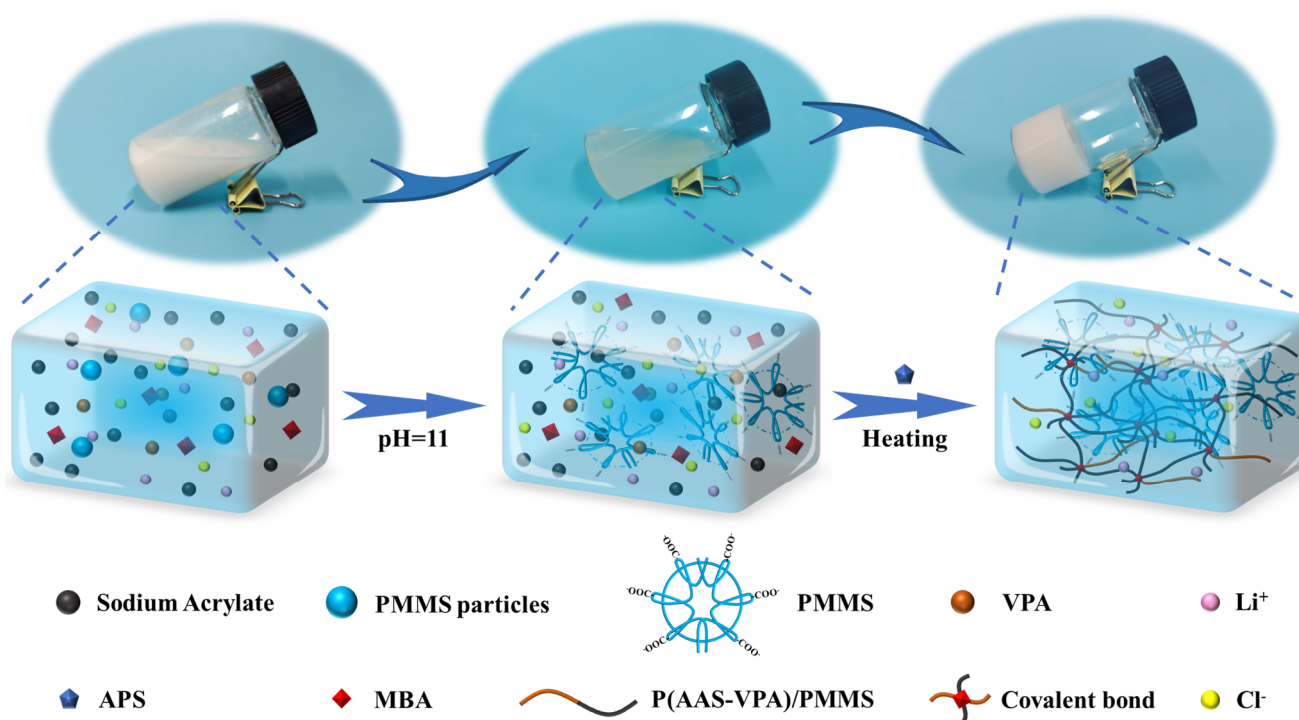
2. Materials and Methods

2.1. Materials

Sodium acrylate (AAS, $>95\%$), vinyl phosphonic acid (VPA, $>95\%$), and anhydrous lithium chloride (LiCl , 99%) were purchased from Macklin Biochemical Technology Co., Ltd., (Shanghai, China). N,N' -Methylene bisacrylamide (MBA, AR), ammonium persulfate (APS, AR), tetramethylethylenediamine (TEMED, 99%), and Aniline (ANI, 99.5%) were purchased from Aladdin Chemical Co., Ltd., (Shanghai, China). Sodium hydroxide (NaOH) was purchased from Colon Chemicals Co., Ltd., (Chengdu, China). Perchloric acid (HClO_4 , AR) was purchased from Sinopharm Chemical Reagent Co., Ltd., (Shanghai, China). PMMS was synthesized according to the previous report [19] in our group. All the reagents were used with no further purification. The water used for the experiments was deionized water.

2.2. Preparation of the P(AAS-VPA)/PMMS Composite Hydrogel

The P(AAS-VPA)/PMMS composite hydrogel was prepared via free radical polymerization. As shown in Scheme 1, firstly, sodium acrylate, VPA, MBA, and dispersed PMMS particles were added into 40 *w/v*% of LiCl solution and stirred to form a uniform mixture. Second, NaOH solution was added drop by drop to adjust the pH value to 11 with vigorous stirring. After dripping, stirring was continued for 3 h to ensure the complete transformation of the PMMS particles into the copolymer clusters (Figure S1). Finally, the set amount of APS was added, and the mixture was quickly injected into a cylindrical glass mold measuring 26 mm in diameter and 20 mm high and placed at 60 °C for 10 h to obtain the stable P(AAS-VPA)/PMMS composite hydrogel.



Scheme 1. Schematic diagram of the preparation of the P(AAS-VPA)/PMMS composite hydrogel.

2.3. Fabrication of Supercapacitors

The preparation of supercapacitors referred to the method reported in the literature. An amount of 93 mg (1 mmol) of aniline was added into 40 mL of perchloric acid solution ($V_{\text{perchloric acid}}:V_{\text{water}} = 1:11$), and 59 mg (0.26 mmol) of APS was dissolved in 10 mL of the same proportion of perchloric acid solution at 0 °C. The P(AAS-VPA)/PMMS composite hydrogel was immersed in prepared aniline solution for 0.5 h before the APS solution was added, and then it was stirred continuously for 24 h at room temperature to ensure the formation of a complete PANI layer on the surface of the hydrogel. Then, the edges of the hydrogel with the PANI layer were cut off, and a sandwich-like supercapacitor was fabricated.

To investigate the effect of the thickness of the PANI layer on the sandwich-like supercapacitor, different concentrations of aniline solutions (93 mg, 186 mg, and 279 mg) and corresponding supercapacitors were prepared and named as follows: SuperC-1, SuperC-2, and SuperC-3. Carbon cloth electrodes and platinum wires were employed to measure the electrochemical performance of the supercapacitor assembled by the P(AAS-VPA)/PMMS composite hydrogel with the PANI layer, and the hydrogel was cut into a cuboid measuring 40 mm in length, 15 mm in width, and 3 mm in height.

2.4. Characterization Testing

2.4.1. Mechanical Performance Test

Tensile test: For the tensile test, the hydrogel samples were prepared into dumbbell-shaped samples with a length of 20 mm, a width of 4 mm, and a thickness of 2 mm in PTFE molds. The hydrogels were stretched at a uniform rate of 500 mm/min on a UTM 2202 universal testing machine with a maximum load of 200 Nm. Each sample was tested three times in a parallel manner. The modulus of elasticity was defined as the slope of the initial linearity of the stress–strain curve. Toughness was calculated from the integral area of the stress–strain curve; meanwhile, the dissipative energy was defined as the difference between the integral area of the loading curve and that of the unloading curve. In addition, cyclic tensile testing was carried out at a tensile speed of 200 mm/min.

Compression test: The sample size was a 16 mm diameter cylindrical hydrogel. The hydrogel samples were subjected to single and cyclic compression at a compression rate of 3 mm/min on a UTM2202 universal testing machine with a load of 200 N. Each hydrogel sample was tested at least three times in parallel.

2.4.2. Adhesion Performance Test

The hydrogel sample was made into a sheet measuring 110 mm in length, 15 mm in width, and 3 mm in height, and subjected to a 90° adhesion peel test with a UTM2202 universal testing machine at a speed of 100 mm/min. Before the testing, the backside of the hydrogel sample was immobilized on a polyurethane film to restrict its distortion along the tensile direction; the alternative side was firmly adhered to the substrate under test (rubber, aluminum sheet, plastic, and polytetrafluoroethylene). Prior to testing, a weight of about 800 g was put on the samples and held for 10 min in order for the hydrogel samples to strongly adhere to the surface of the substrate. Each sample was tested at a minimum of six parallel times and the averages were calculated.

2.4.3. Conductivity Test

The ionic conductivity of the hydrogels was investigated via electrochemical impedance spectroscopy (EIS). The hydrogel was placed between two nickel foam electrodes and impedance data were collected with a CHI660E electrochemical workstation in the frequency range from 10^5 Hz to 10^{-2} Hz at 25 °C. The conductivity of the hydrogel was calculated according to the following Equation (1):

$$\delta = L / (R_b \times S) \quad (1)$$

The thickness is L , R_b is the volume resistance, which is obtained from the impedance data, and S is the area of contact between the hydrogel and the electrode. We repeated the test at least six times for each sample and the average value was taken.

2.4.4. Sensing Performance Test

The P(AAS-VPA)/PMMS hydrogel was assembled into a simple strain sensor by connecting two wires directly to it, and the sensing performance was tested by applying the hydrogel parts directly to the fingers, wrist, elbow, knee, and throat of the volunteer, respectively. The experimental voltage at 0.03 V was fixed, and the current changes during human joint movements as well as speech and swallowing were monitored with a CHI660E electrochemical workstation. The evaluation of the sensing performance of the hydrogel was performed according to the following Equation (2):

$$\Delta I / I_0 = [(I - I_0) / I_0] \times 100\% \quad (2)$$

The I and I_0 represent the immediate current values of the hydrogel when strain is applied and when no strain is imposed, respectively.

In addition, hydrogels were characterized for strain sensing sensitivity by measuring the resistance values of hydrogels under different tensile strains. The strain sensitivity is calculated according to the following Equation (3):

$$GF = [(R - R_0)/R_0]/\varepsilon \quad (3)$$

where R and R_0 are the values of the resistance of the hydrogel before and after the stretching, respectively, and ε is the imposed strain.

2.4.5. Capacitance Performance Characterization

The performance of the supercapacitor with a two-electrode structure was evaluated using electrochemical impedance spectroscopy (EIS), cyclic voltammetry (CV), and constant current charge/discharge (GCD) techniques with a CHI660e electrochemical workstation (Tatsuhwa Instruments Co., Ltd., China).

In addition, the supercapacitors were kept at $-30\text{ }^\circ\text{C}$, $0\text{ }^\circ\text{C}$, and $25\text{ }^\circ\text{C}$ for 12 h before performing low-temperature electrochemical measurements. The specific capacitances reported in this study are all area-specific capacitances of the electrodes.

The area-specific capacitance (C_A , $\text{mF}\cdot\text{cm}^{-2}$) of the supercapacitor was calculated according to Equation (4):

$$C_A = 2 \cdot I \cdot \Delta t / (A \cdot \Delta V) \quad (4)$$

where I , Δt , A , and ΔV represent the discharge current (mA), the discharge time (s), the area of the hydrogel electrolyte (cm^2), and the changing voltage (V) during the discharge, respectively.

The energy density (E_A , $\mu\text{Wh}\cdot\text{cm}^{-2}$) of the supercapacitor was calculated according to Equation (5):

$$E_A = \frac{1}{2} \cdot C_A \cdot \Delta V^2 \cdot \frac{1000}{3600} \quad (5)$$

The power density (P_A , $\mu\text{W}\cdot\text{cm}^{-2}$) of the supercapacitor was calculated according to Equation (6):

$$P_A = E_A / \Delta t \quad (6)$$

3. Results and Discussion

3.1. The Preparation of the P(AAS-VPA)/PMMS Composite Hydrogel

In this work, we selected sodium acrylate (AAS) as the major monomer, ethylene phosphoric acid (VPA) as the co-monomer, and a small amount of MBA as the crosslinking agent; the polyelectrolyte network of P(AAS-VPA) was formed through radical polymerization. PAAS is a well-known environment-friendly polyelectrolyte commonly used as a water treatment agent to complex toxic metal ions and is used as a surfactant or thickener in foods to enhance the protein viscosity in raw starch and the viscoelasticity of food. VPA is a non-toxic, water-soluble functional monomer; the phosphonic acid group of VPA is universal adhesion [20]. VPA can adhere to diverse substrates, and has the function of promoting cell adhesion and proliferation; as such, VPA is often used as an important component in biomaterials for cell culture and tissue repair [21]. The addition of VPA can also enhance the mechanical properties and ionic strength of materials [22]. PMMS is referred to as poly(methacrylic acid–methyl methacrylate), which is a soft tissue repair material [23]. Here, PMMS is used as a physical crosslinked network to increase the toughness and deformation recoverability of polyelectrolyte hydrogels.

3.2. Flexibility and Recoverability of the P(AAS-VPA)/PMMS Composite Hydrogel

Flexibility and recoverability are two important factors to evaluate whether conductive hydrogels can be used as flexible sensors or supercapacitors. As shown in Figure 1b, the P(AAS-VPA)/PMMS composite hydrogel can still maintain integrity after being stretched to five times the original length. It can also withstand various types of deformation such as knotting, stretching after knotting, and bending in half. Even after being uniaxially

compressed to 1/5 of its original height, it would immediately return to its original height once unloaded. These results show that the P(AAS-VPA)/PMMS composite hydrogel has excellent elasticity and toughness. The tensile test results showed that the P(AAS-VPA)/PMMS composite hydrogel achieved a high tensile strength of 0.56 MPa with a maximum elongation of 2100%, (Figure 1d); meanwhile, the hydrogel demonstrated a high compressive modulus of 0.83 MPa (Figure 1g).

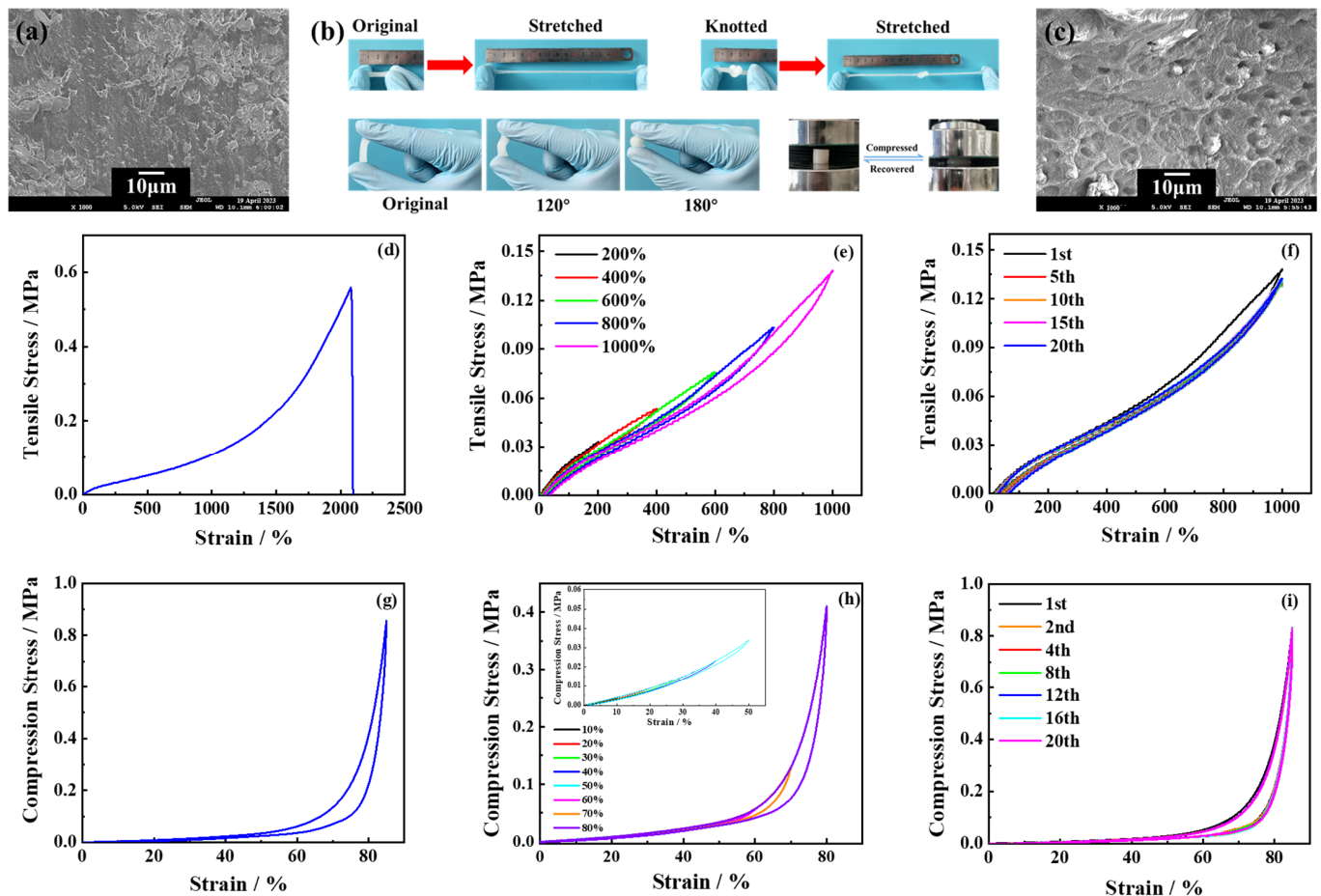


Figure 1. Mechanical properties of the P(AAS-VPA)/PMMS composite hydrogel: (a) SEM image of the initial lyophilized hydrogel; (b) optical photographs of the hydrogels under tensile, knotting, bending, and compression; (c) SEM image of the lyophilized hydrogel stretched to 7 times the initial length; (d) tensile stress–strain curve; (e) tensile loading–unloading curves at different strain% (200, 400, 600, 800, and 1000); (f) 20 consecutive cycles of tensile loading–unloading at 1000% of strain; (g) compressive stress–strain curve; (h) compression loading–unloading curves at different strain% (10, 20, 30, 40, 50, 60, 70, and 80); and (i) 20 consecutive cycles of compression at 85% of the strain.

To explore the fatigue resistance and deformation recoverability of the P(AAS-VPA)/PMMS composite hydrogel, cyclic tensile and compression tests were also conducted. The loading–unloading experimental results at different tensile strains (Figure 1e) showed that the dissipation energy represented by the hysteresis loop area was magnified significantly with the strain increasing from 200% to 1000%. A total of 20 consecutive cyclic loading–unloading tests at 1000% of the tensile strain were conducted. The results show that except for the obvious hysteresis loop in the first loading–unloading cycle, the hysteresis loops were very small and highly overlapping in the subsequent loading–unloading cycles (Figure 1f). During the first loading–unloading experiment, the internal structure of the prepared hydrogel was not complete and some intermolecular interactions and even chemical bonds were destroyed; as a result, after unloading, some energy was dissipated.

In the subsequent loading–unloading cycles, the physical entanglement between PMMS clusters played a role in maintaining the stability of the gel network structure to maintain the hydrogel's good tensile deformation recoverability and fatigue resistance.

The results of the compression stress–strain curve and compression loading–unloading cycle experiments of the P(AAS-VPA)/PMMS composite hydrogel are similar to those of the tensile tests (Figure 1h,i). The hysteresis loops enlarged with compression strain, increasing from 10 to 80%. Setting the compression strain at 85%, the results of 20 cyclic compression loading–unloading experiments showed that except for the first cycle, the hysteresis loops of all other cycles basically overlapped. It was further confirmed that the P(AAS-VPA)/PMMS composite hydrogel has excellent deformation recoverability and fatigue resistance.

In order to observe whether the internal structure of the P(AAS-VPA)/PMMS hydrogel is broken, SEM was conducted on the stretched hydrogel sample. After being stretched to seven times the initial length, the hydrogel was immediately immersed in liquid nitrogen to freeze. It was observed via SEM after freeze drying. Compared with the initial hydrogel (Figure 1a), after being stretched, the hydrogel exhibited an obvious tensile orientation (Figure 1c), but no micro-fracture was observed under a magnification of 1000 times, which indicates that the hydrogel has very good tensile deformation ability and structural stability.

3.3. Adhesion Properties of the P(AAS-VPA)/PMMS Composite Hydrogel

It is well known that suitable self-adhesive force is very important for conductive hydrogels to ensure that mechanical signals are stably converted into electrical signals [24]. In this work, VPA units introduced into the conductive hydrogel system not only effectively enhanced the mechanical properties of the hydrogel, but also imparted self-adhesive properties to the hydrogel. As shown in Figure 2a,b, the P(AAS-VPA)/PMMS composite hydrogel can firmly adhere to various substrates such as metal, glass, plastic, wood, rubber, and so on. By reason of the self-adhesive force, the cylindrical hydrogel sample with a diameter of 1 cm can easily lift a 480 g weight or other objects. In addition, the P(AAS-VPA)/PMMS composite hydrogel also showed considerable adhesion properties to skin tissues.

To further investigate the adhesion properties, the adhesion effect of the hydrogel on different substrates was investigated via the 90° peeling method (Figure 2c,d). The hydrogel showed differential adhesion strength to different substrates, for example, 128 N/m to PTFE, 191.2 N/m to an aluminum plate, 256 N/m to epoxy resin, and 384 N/m to silicon rubber.

These results are mainly due to the fact that the P(AAS-VPA)/PMMS composite hydrogel contains a large number of carboxylate groups, phosphonic hydroxyl groups, ester groups, and hydrophobic carbon chains, which can form different interactions, such as hydrogen bonds, coordination bonds, dipole–dipole interactions, and so on. Between the hydrogel and the substrates, especially, the phosphonic groups in the VPA units have been widely considered to form hydrogen bonding interactions, ionic bonding interactions, dipole–dipole interactions, and other interactions with different groups [20], for example, forming ionic bonding interactions and dipole–dipole interactions with the aluminum plate.

More importantly, the hydrogel has a reversible adhesion property on the surface of the matrix, which is different from the irreversible adhesion of the traditional tape. Here, 90° adhesion peel cyclic tests were conducted using an aluminum plate as the substrate. The results (Figure 2e) showed that the P(AAS-VPA)/PMMS composite hydrogel exhibited excellent reversible adhesion properties during the experiments, and the adhesion strength of 10 cycles varied between 180 N/m and 190 N/m. Considering operational errors, the P(AAS-VPA)/PMMS composite hydrogel almost maintains the original peeling adhesion strength, which indicates that reversible and lasting adhesion can be achieved between the hydrogel and the metal aluminum substrate through dynamic interactions. This durable

and excellent adhesion performance lays a solid foundation for the application of P(AAS-VPA)/PMMS composite hydrogels in artificial intelligence and biomedical fields.

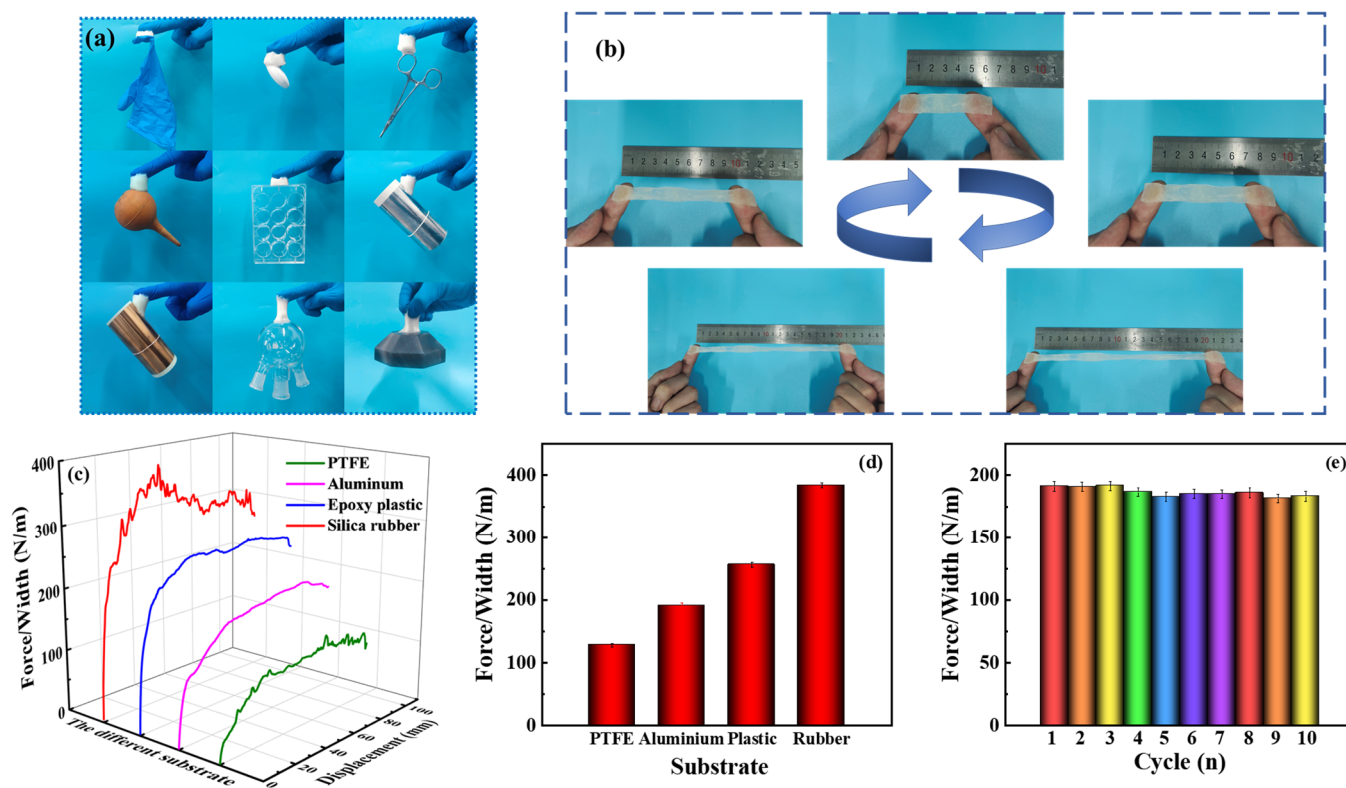


Figure 2. Adhesion performance of the P(AAS-VPA)/PMMS composite hydrogel: (a) optical photographs of the hydrogel adhering to different substrates; and (b) optical photographs of the performance of the hydrogel adhering to the fingers and experiencing a loading–unloading tensile cycle on the fingers; (c) 90° adhesion peel test of the hydrogel on different substrates (PTFE, aluminum plate, plastic, and rubber); (d) the corresponding adhesion peeling strengths; and (e) 10 cycles of adhesion peeling strength tests using aluminum sheet as the sample substrate.

3.4. Sensing Properties of the P(AAS-VPA)/PMMS Composite Hydrogel

As shown in Figure 3a, when the composite hydrogel was connected to a closed circuit containing a diode (LED), the LED bulb was successfully lit. This indicates that the ionic hydrogel of P(AAS-VPA)/PMMS has the function of conducting electricity. The ionic conductivity of the P(AAS-VPA)/PMMS hydrogel was carefully investigated via electrochemical impedance spectroscopy (EIS) (Figure 3b). It is generally believed that in the Nyquist plot in the EIS, the semicircle under high frequency reflected the charge transfer resistance and the straight lines under low frequency reflected the charge diffusion process [25]. Controlled by the charge diffusion, the Nyquist plot of the P(AAS-VPA)/PMMS hydrogel presented a straight line, and the slope was higher than 45°, possibly because of the interface capacitance [26]. According to the Nyquist plot and Formula (1) $\delta = L / (R_b \times S)$, the calculated ionic conductivity of the optimized P(AAS-VPA)/PMMS composite hydrogel achieved a value as high as 0.045 S·cm⁻¹.

The excellent deformation recoverability, fatigue resistance, universal adhesion, and outstanding ionic conductivity of the P(AAS-VPA)/PMMS composite hydrogel provide an opportunity for its application as a strain sensor. Therefore, the sensing performance of the composite hydrogel was preliminarily investigated at different strains. The strain sensing performance was evaluated according to the change in relative current ($\Delta I/I_0$, the change in strain causes the change in hydrogel resistance and, further, the change in current) (Figure 3c). The $\Delta I/I_0$ value increased with increasing tensile strain; meanwhile,

for the same strain, the $\Delta I/I_0$ value reversibility changed with loading–unloading cycles. These results indicate that the P(AAS-VPA)/PMMS composite hydrogel can be applied to strain sensors and is capable of monitoring and differentiating strain changes with high reliability.

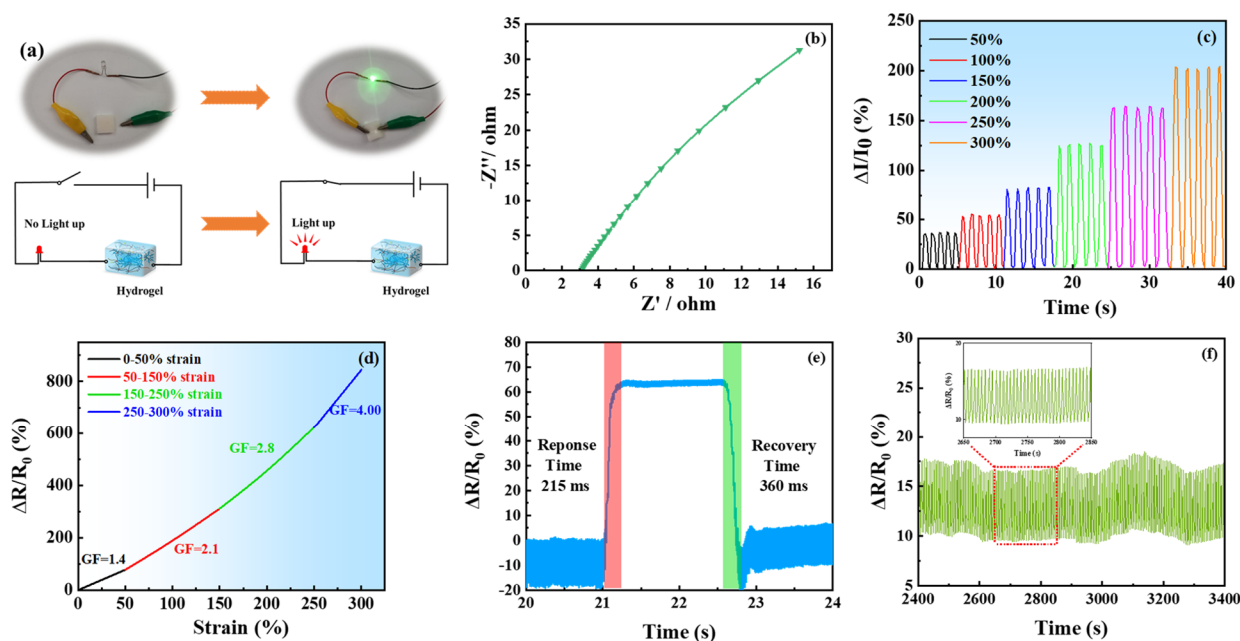


Figure 3. Sensing properties of the P(AAS-VPA)/PMMS composite hydrogel: (a) optical photographs of the hydrogel connected to a closed circuit to light a diode; (b) EIS of the hydrogel with the frequency varying between 10^5 Hz and 10^{-2} Hz; (c) strain sensing performance of the hydrogel under different tensile deformations; (d) sensitivity factor (GF) of the hydrogel for the strain sensor in the range of 0–300% of the strain; (e) response and recovery times of the hydrogel sensor with tensile strain loading–unloading; and (f) 1000 consecutive cycles of tensile loading–unloading at 100% of the strain.

The $\Delta R/R_0$ (i.e., $GF = [(R - R_0)/R_0]/\varepsilon$) was commonly used to represent the sensing sensitivity in the literature [27,28]. The $\Delta R/R_0$ values increased almost linearly with the strain in the range of 0–300% (Figure 3c). The GF value gradually increased from 1.4 at low strains (0–50%) to 2.0 at medium strains (~150%), and then to 4.0 at the higher strain (300%), which indicates that the P(AAS-VPA)/PMMS composite hydrogel has a high degree of strain sensitivity, even when subjected to a tiny strain.

In addition, the hysteresis behavior of hydrogel sensing was also studied. Taking into account the large hysteresis loop in the first cyclic tensile test in Figure 1d, before the preparation of the strain sensor, the P(AAS-VPA)/PMMS composite hydrogel samples were treated with one cyclic tensile. We found that the response and recovery times of the hydrogel were 215 ms and 360 ms, respectively, within a loading–unloading cycle (Figure 3e). Moreover, 1000 consecutive tensile cycles were conducted and no evident signal degradation was observed (Figure 3f), which indicates that the P(AAS-VPA)/PMMS composite hydrogel sensor has very high sensitivity and responsiveness and has great potential for real-time monitoring of the full range of human activities.

Because of the excellent adhesion property of the P(AAS-VPA)/PMMS composite hydrogel, it can be easily attached to different locations on the human body, such as fingers, wrists, larynx, knee joints, and other areas with complex shapes. Figure 4a–d show that P(AAS-VPA)/PMMS composite hydrogel sensors adhered to the joint parts of fingers, wrists, arms, and knees, respectively, to monitor the $\Delta I/I_0$ value changes during recurrent joint movements. Whether the bending motion of small joints, such as the finger joint (Figure 4a) and wrist joint (Figure 4b), or the bending motion of large joints, such as the elbow joint (Figure 4d) and knee joint (Figure 4c), the same bending degree demonstrated

the same $\Delta I/I_0$ value in cyclic bending movements, and the $\Delta I/I_0$ curves exhibited periodic repetition with the motion frequency. Interestingly, different joint movements formed different peaks at the $\Delta I/I_0$ curves, which further explains the unique sensitivity of the P(AAS-VPA)/PMMS composite hydrogel sensor.

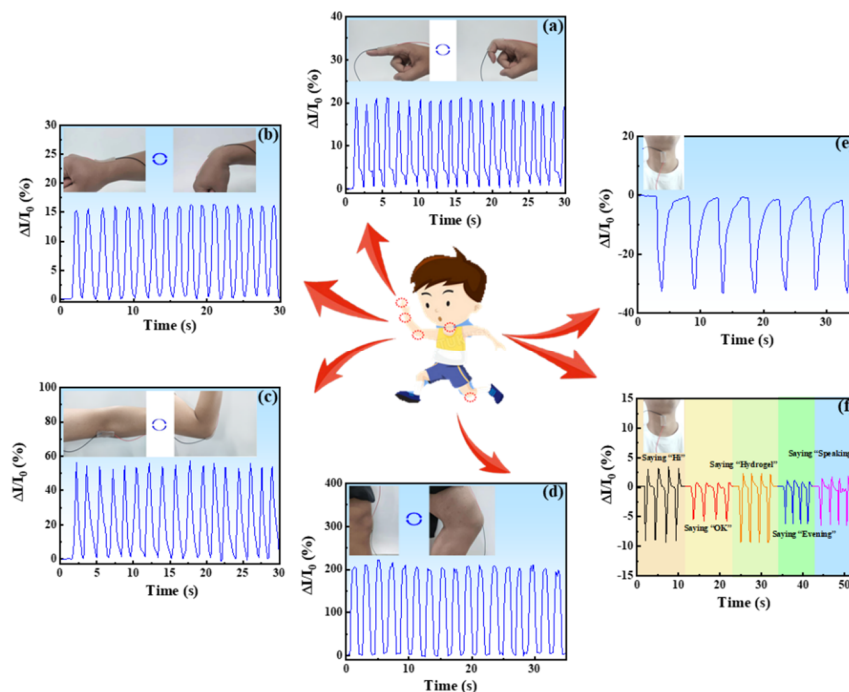


Figure 4. Sensing performance of the P(AAS-VPA)/PMMS composite hydrogel for real-time monitoring of human joint movements and physiological activities: (a) finger bending; (b) wrist bending; (c) elbow bending; (d) knee bending; (e) throat swallowing; and (f) throat vocalization.

More importantly, P(AAS-VPA)/PMMS composite hydrogel-based strain sensors can not only accurately distinguish and monitor relatively large joint bending or relaxation movements, but also efficiently and stably monitor small amplitude strains (such as swallowing movements and throat vocalizations). As shown in Figure 4e,f, the P(AAS-VPA)/PMMS composite hydrogel strain sensors were capable of stably monitoring swallowing movements, as well as vocalizations, such as speaking the words “Hi”, “OK”, “hydrogel”, “evening”, and “speaking”. Different words have different $\Delta I/I_0$ values and peak curves, so the P(AAS-VPA)/PMMS composite hydrogel sensor can accurately transmit voice information. Therefore, the P(AAS-VPA)/PMMS composite hydrogel strain sensor shows a promising application for wearable electronic devices to monitor human movement and health.

From the sensing signals, it can be seen that the P(AAS-VPA)/PMMS composite hydrogel sensor has obvious sensing hysteresis behavior. This hysteresis behavior is due to the typical viscoelastic behavior of the hydrogel, which can eventuate signal hysteresis and fluctuations, leading to a decrease in sensing performance [29]. The analysis of the composition of the P(AAS-VPA)/PMMS hydrogel showed that it contains PMMS clusters and VPA structural units. PMMS clusters provide the hydrogel with plastic deformation ability, but they delay the elastic recovery of the hydrogel (Figure S3a–c). VPA structural units enhance the adhesion behavior of the hydrogel, but they also increase the viscosity of the hydrogel and further delay the elastic recovery.

3.5. Capacitive Properties of the P(AAS-VPA)/PMMS Composite Hydrogel

An ionic conductive hydrogel with excellent recoverability, flexibility, and ionic conductivity is an ideal quasi-solid electrolyte for assembling a flexible supercapacitor [30]. In this work, a P(AAS-VPA)/PMMS composite hydrogel with optimized composition as

a quasi-solid electrolyte was selected to construct a simple “sandwich” supercapacitor consisting of the P(AAS-VPA)/PMMS composite hydrogel with polyaniline deposited on the surfaces, with the edges cut off to avoid short circuit (Figure 5a), and two pieces of carbon cloth tightly attached to the upper and lower surfaces. The cross-sectional photo clearly presents the deposition and penetration of polyaniline onto the P(AAS-VPA)/PMMS composite hydrogel. The structure of the P(AAS-VPA)/PMMS composite hydrogel with polyaniline deposited on the surfaces was confirmed by the observation results obtained via optical microscope and SEM (Figure 5b,c).

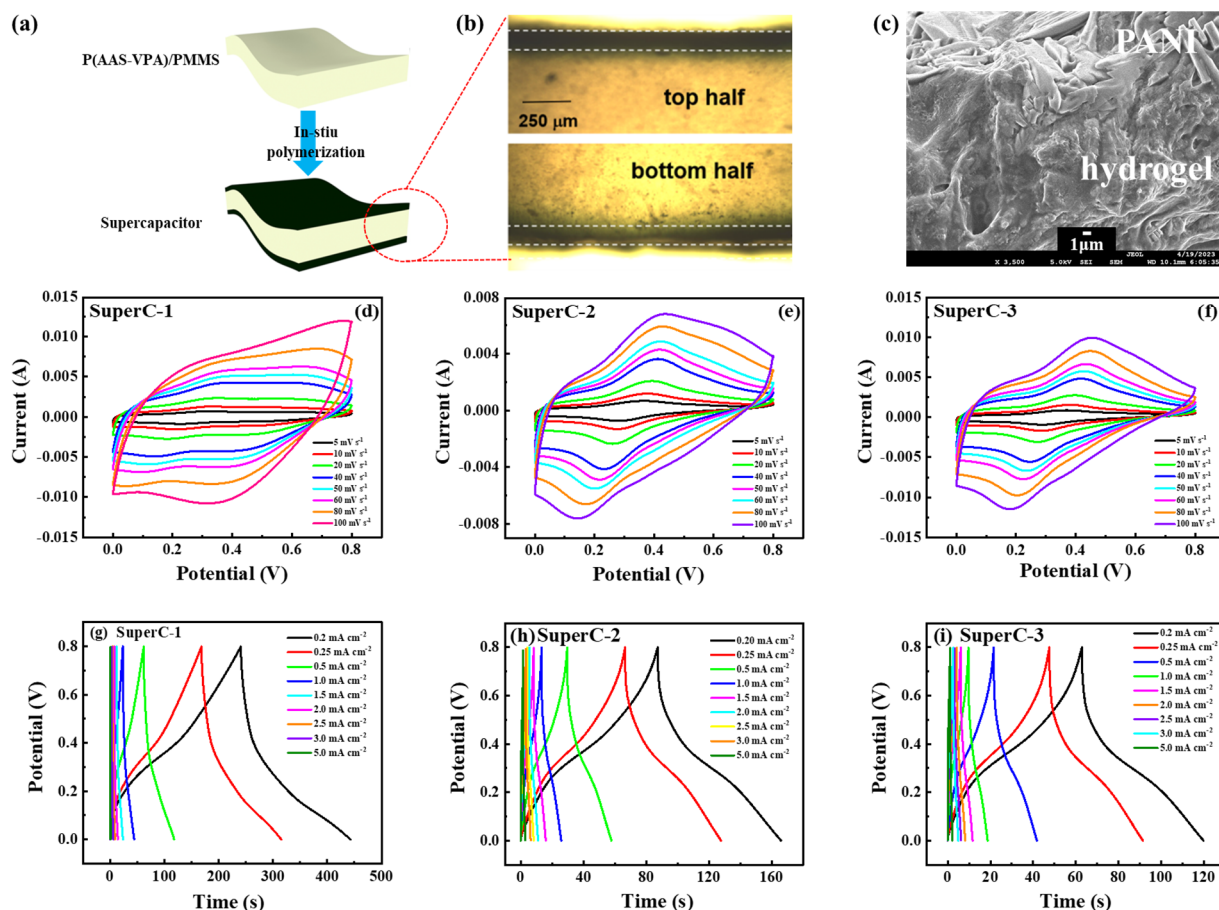


Figure 5. Capacitive performance of the P(AAS-VPA)/PMMS composite hydrogel at different PANI depositions: (a) Schematic cross-section of the hydrogel/PANI capacitor; (b) optical microscope image and (c) the cross-sectional SEM image of the in situ generated polyaniline layer on the hydrogel electrolyte; (d–f) CV curves of SuperC-1, SuperC-2, and SuperC-3 with the scanning rate changing from $5 \text{ mV}\cdot\text{s}^{-1}$ to $100 \text{ mV}\cdot\text{s}^{-1}$, respectively; and (g–i) GCD curves of SuperC-1, SuperC-2, and SuperC-3 at a current density range of 0.2 to $5.0 \text{ mA}\cdot\text{cm}^{-2}$.

The electrochemical properties of supercapacitors were characterized using cyclic voltammetry (CV), constant current charge–discharge (GCD), electrochemical impedance spectroscopy (EIS), and cycling stability.

As seen from Figure 5d–f, the CV curves of all of the P(AAS-VPA)/PMMS hydrogels with different PANI depositions, named SuperC-1, SuperC-2, and SuperC-3, show significant redox peaks within the scanning rate variation range of 5 to $100 \text{ mV}\cdot\text{s}^{-1}$, which is due to the typical pseudocapacitive behavior of PANI [31]. The capacitive performances of SuperC-1, SuperC-2, and SuperC-3 were also performed via the GCD curve evaluation at the current density range of 0.2 to $5.0 \text{ mA}\cdot\text{cm}^{-2}$ (Figure 5g–i). All of the GCD curves were approximately triangular, which is the typical performance of a double-layer capacitor [31].

In order to compare the effect of polyaniline on the electrochemical properties of supercapacitors, using the drying and gravimetric method, the loading mass of the polyaniline of the supercapacitors was calculated by the deposition amount of polyaniline per square centimeter of hydrogel surface. There was $3.43 \text{ mg}\cdot\text{cm}^{-2}$ of polyaniline on the surface of SueperC-1, $4.25 \text{ mg}\cdot\text{cm}^{-2}$ on that of SueperC-2, and $6.61 \text{ mg}\cdot\text{cm}^{-2}$ on that of SueperC-3, respectively.

The transport process of the charge in the device can be studied by the EIS (Figure 6a). The intercept on the Z' axis in the Nyquist plot indicates the capacitor resistance. As the aniline content increases, it makes the aniline-containing layer containing the hydrogel electrolyte loaded by the hydrogel thicker, causing the distance between the two electrode sheets to decrease, which makes the diffusion resistance decrease and shows an increase in the slope of the curve in the Figure, as shown in Figure 6a [32].

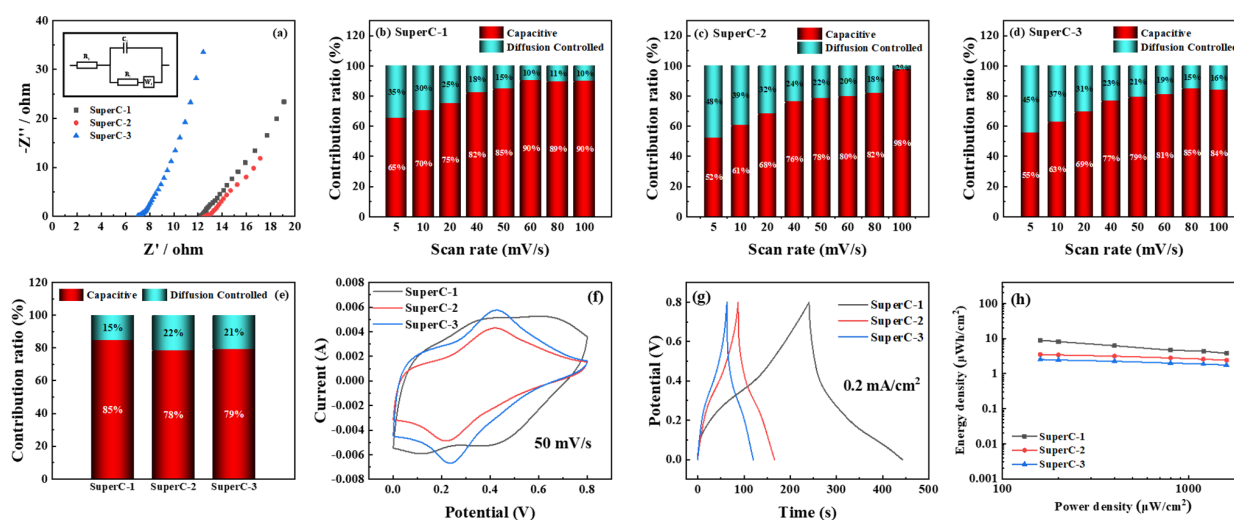


Figure 6. (a) EIS of SuperC-1, SuperC-2, and SuperC-3; (b–d) histograms representing the contribution ratio of capacitance and diffusion control to charge storage in SuperC-1, SuperC-2, and SuperC-3 under different sweep speeds, respectively; (e) comparison of the contribution of capacitive and diffusion control with the charge storage at a scan rate of $50 \text{ mV}\cdot\text{s}^{-1}$; (f) CV curves at a scan rate of $50 \text{ mV}\cdot\text{s}^{-1}$; (g) GCD curves at a current density of $0.2 \text{ mA}\cdot\text{cm}^{-2}$; and (h) Ragone plots.

There are two main mechanisms of energy storage for a similar CV curve as in Figure 5d–f: one is a Faraday process, which can also be called a Faraday contribution (redox reaction occurs), and the other is a non-Faraday process, which can similarly be called a non-Faraday contribution (reversible charge storage for double-layer capacitance) [33–35]. In order to understand the electron storage mechanism in our supercapacitor, the relationship between the peak current (i_p) and its scan rate (v) in the GCD curve is analyzed according to Equation (7):

$$i_p = av^b \quad (7)$$

where a and b are variables.

Taking Equation (7) into logarithmic form yields Equation (8):

$$\text{Log}i_p = b\text{Log}v + \text{Log}a \quad (8)$$

The different scan rates and their corresponding peak currents were brought into Equation (8), and their scatter plots were drawn with $\text{Log}v$ and $\text{Log}i_p$ as the independent and dependent variables. The data were linearly fit with OriginLab to derive the values of a and b .

According to the analysis in Mr. Bruce Dunn's article [36], the observed SuperC b values are between 0.5 and 1.0, which indicates a mixture of diffusion control and capacitance-like responses.

To further quantify the capacitance contribution of capacitance and diffusion limitations to all SuperCs, the CV curves of all SuperCs were further analyzed according to Equation (9):

$$i_V = k_1 v + k_2 v^{1/2} \quad (9)$$

where i_V is the current at the selected scan speed, $k_1 v$ is the contribution of the surface capacitance effect to the overall capacitor current, and $k_2 v^{1/2}$ is the contribution of the diffusion-controlled intercalation process.

The capacitance contributions and controlled-diffusion contributions of SuperC-1, SuperC-2, and SuperC-3 at different scan rates are shown in Figure 6b–d. It can be seen that the capacitance of all SuperCs is overwhelmingly provided by the surface capacitance, and their capacitance contribution values are close to 1 during the scan rate of $60 \text{ mV}\cdot\text{s}^{-1}$ – $100 \text{ mV}\cdot\text{s}^{-1}$, indicating that the charge storage of all SuperCs is mainly capacitive within the range. Compared at $50 \text{ mV}\cdot\text{s}^{-1}$ scanning speed (Figure 6e), it is easy to see that the area capacitance contribution of SuperC-1 is the largest, which demonstrates its excellent capacitance dominance characteristics.

The CV curves of SuperC-1, SuperC-2, and SuperC-3 at a scan rate of $50 \text{ mV}\cdot\text{s}^{-1}$ and GCD curves at a current density of $0.2 \text{ mA}\cdot\text{cm}^{-2}$ were selected for comparison of the influence of the loading mass of PANI with the electrochemical performance of the hydrogel capacitors (Figure 6f,g). In Figure 6f, we can clearly see that the integrated area of SuperC-1 was larger than those of SuperC-2 and SuperC-3, which indicates that SuperC-1 has a higher specific capacitance. The discharge time of SuperC-1 was much longer than those of SuperC-2 and SuperC-3 and, as shown in Figure 6h, the energy density of SuperC-1 is the highest, and the energy density of SuperC decreases instead with the increase in the added aniline content. The reason for these results may be because the excessive polyaniline forms a tighter fiber network on the surface of the hydrogel to prevent the free movement of charge and, as a result, the capacitive performance of the hydrogel electrolyte is reduced.

The electrochemical properties of SuperC-1 under different deformations are shown in Figure 7a,b, which show the CV curves with a sweep speed of $20 \text{ mV}\cdot\text{s}^{-1}$ and the GCD curves with $1 \text{ mA}\cdot\text{cm}^{-2}$ under different deformations (bending 0° , 90° , 180° , twisting 90° , and finger pressure), respectively, and the results show that the GCD curves and CV curves under strain do not change much, indicating that the capacitor had almost no capacity loss. The GCD test of SuperC-1 was continued 10,000 times and the calculated coulombic efficiency was plotted. The coulombic efficiency was stable at about 97.7% after 10,000 cycles. It can be seen that the all-in-one SuperC-1 supercapacitor in this paper has good electrochemical stability and structural stability [37]. This result may be due to the fact that the SuperC-1 supercapacitor is all-in-one molded and a part of the polyaniline in the electrode material is physically entangled with the hydrogel electrolyte, and the light green layer between the polyaniline and the hydrogel electrolyte, i.e., the P(AAS-VPA)/PMMS and the polyaniline layer, can be clearly observed in Figure 5b,c.

In addition, the temperature dependence of the electrochemical properties of the P(AAS-VPA)/PMMS hydrogel electrolyte was characterized via CV and GCD in the temperature range of -30°C to 25°C . As shown in Figure 8a,b, the CV and GCD curves' integral area gradually reduced with a decrease in temperature. These phenomena can be explained by the restricted migration of charge ions at low temperatures. The P(AAS-VPA)/PMMS hydrogel electrolyte had an excellent high area capacitance of $100.8 \text{ mF}\cdot\text{cm}^{-2}$ and energy density of $8.96 \text{ }\mu\text{Wh}\cdot\text{cm}^{-2}$ at room temperature (Figure 8c). Meanwhile, even at -30°C , the hydrogel electrolyte still has a high area capacitance of $25.3 \text{ mF}\cdot\text{cm}^{-2}$ and energy density of $2.25 \text{ }\mu\text{Wh}\cdot\text{cm}^{-2}$, which indicates that the flexible supercapacitor based on the P(AAS-VPA)/PMMS composite hydrogel electrolyte can be applied not only at room temperature but it can also be adapted to lower temperatures, which greatly highlights the fact that the P(AAS-VPA)/PMMS composite hydrogel has a competitive edge in the development of "all-in-one" wearable electronic devices.

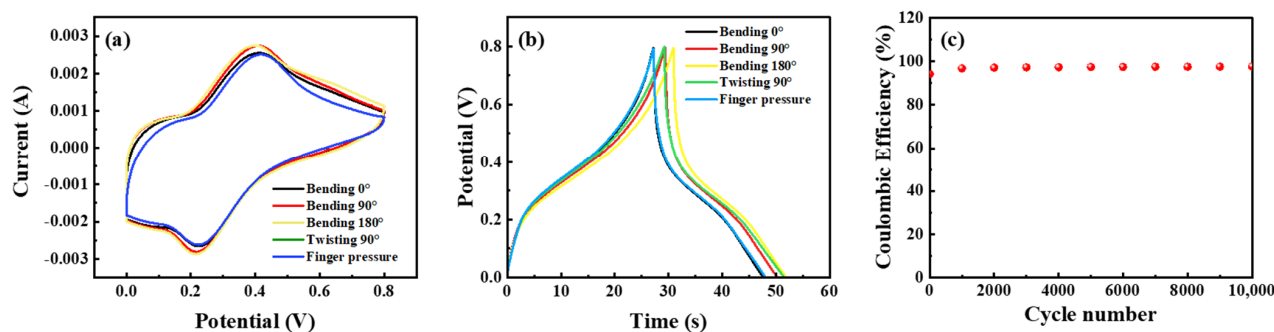


Figure 7. (a) CV curves at a scan rate of $20 \text{ mV}\cdot\text{s}^{-1}$; (b) GCD curves at a current density of $1 \text{ mA}\cdot\text{cm}^{-2}$ under different deformations (bending 0° , 90° , 180° , twisting 90° , and fingertip press); and (c) Coulomb efficiency with 10,000 cycles of GCD at a current density of $3 \text{ mA}\cdot\text{cm}^{-2}$ (SuperC-1 as the sample supercapacitor).

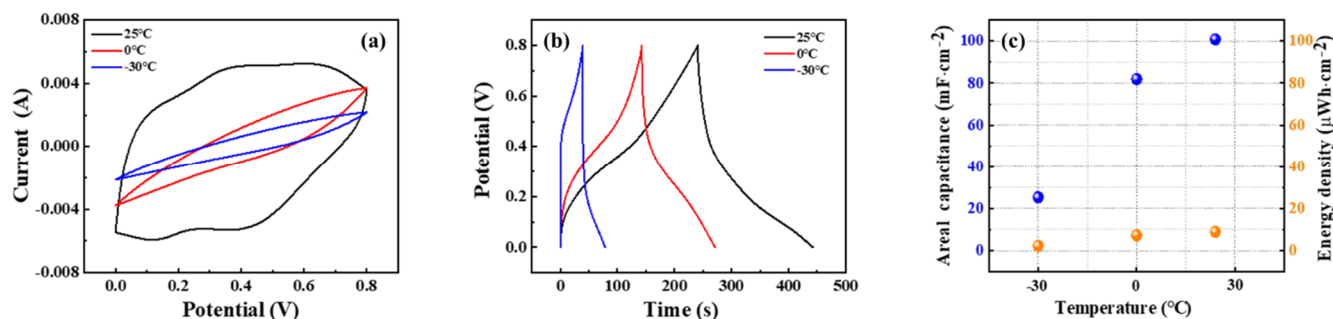


Figure 8. (a,b) CV curves of the P(AAS-VPA)/PMMS hydrogel electrolyte at different temperatures at a $50 \text{ mV}\cdot\text{s}^{-1}$ scan rate and GCD curves at a current density of $0.2 \text{ mA}\cdot\text{cm}^{-2}$, respectively; (c) corresponding area capacitance and energy density.

4. Conclusions

In summary, an ionic conductive hydrogel electrolyte of P(AAS-VPA)/PMMS was prepared using the method of AAS and VPA free radical copolymerization to form a chemically crosslinked network and pH-induced PMMS latex, forming physical cross-linked PMMS clusters. The optimized P(AAS-VPA)/PMMS composite hydrogel has excellent flexibility, deformation recoverability, universal adhesion, conductivity ($0.045 \text{ S}\cdot\text{cm}^{-1}$), and sensing sensitivity ($\text{GF} = 4.0$). The flexible supercapacitor P(AAS-VPA)/PMMS composite hydrogel has excellent capacitance. In addition, the flexible supercapacitor has an area capacitance of -30°C , demonstrating a wide temperature range (area capacitance $100.8 \text{ mF}\cdot\text{cm}^{-2}$ and energy density $8.96 \text{ }\mu\text{Wh}\cdot\text{cm}^{-2}$ at ambient temperature; $25.3 \text{ mF}\cdot\text{cm}^{-2}$ and $2.25 \text{ }\mu\text{Wh}\cdot\text{cm}^{-2}$ at -30°C). The hydrogels have stable electrochemical stability (1000 cycles, coulombic efficiency $> 97\%$) and exhibit electrochemical properties similar to those in the normal state under different deformations. Briefly, we believe that the P(AAS-VPA)/PMMS composite hydrogel has a promising application in the field of flexible quasi-solid electrolytes and sensors.

Supplementary Materials: The following are available online at <https://www.mdpi.com/article/10.3390/batteries9060304/s1>, Figure S1: Schematic diagram of the preparation process, swelling, disentanglement, and regrouping of P(MMA-MAA) latex particles under alkaline conditions. Figure S2: Rheological properties of P(AAS-VPA)/PMMS composite hydrogels. Figure S3: Effect of PMMS and VPA contents on the properties of the P(AAS-VPA)/PMMS composite hydrogels. Figure S4: EIS and conductivity plots for different PMMS contents. Figure S5: Capacitive performance of the P(AAS-VPA)/PMMS composite hydrogel at different PMMS contents. Figure S6: Comparison of CV curves, GCD curves and Rangone for different PMMS contents. Table S1: Comparison of the sensing performance of different hydrogels [17,38–46].

Author Contributions: R.L.: conceptualization, methodology, formal analysis, investigation, funding acquisition, and writing—review and editing; W.L.: formal analysis, data curation, visualization, and writing—original draft preparation; J.C.: investigation, data curation, and visualization; K.F. and J.Z.: writing—review and editing; X.B.: supervision and project administration; X.Z.: conceptualization, methodology, supervision, and funding acquisition. All authors have read and agreed to the published version of the manuscript.

Funding: This research was funded by the National Natural Science Foundation of China (NSFC) (No. 21474092 and No. U1704160).

Data Availability Statement: Not applicable.

Conflicts of Interest: The authors declare no conflict of interest.

References

1. Kwak, S.; Kang, J.; Nam, I.; Yi, J. Free-Form and Deformable Energy Storage as a Forerunner to Next-Generation Smart Electronics. *Micromachines* **2020**, *11*, 347. [[CrossRef](#)]
2. Wang, P.; Hu, M.; Wang, H.; Chen, Z.; Feng, Y.; Wang, J.; Ling, W.; Huang, Y. The Evolution of Flexible Electronics: From Nature, Beyond Nature, and to Nature. *Adv. Sci.* **2020**, *7*, 2001116. [[CrossRef](#)] [[PubMed](#)]
3. Yousaf, M.; Shi, H.T.H.; Wang, Y.; Chen, Y.; Ma, Z.; Cao, A.; Naguib, H.E.; Han, R.P.S. Novel Pliable Electrodes for Flexible Electrochemical Energy Storage Devices: Recent Progress and Challenges. *Adv. Energy Mater.* **2016**, *6*, 1600490. [[CrossRef](#)]
4. Amjadi, M.; Kyung, K.-U.; Park, I.; Sitti, M. Stretchable, Skin-Mountable, and Wearable Strain Sensors and Their Potential Applications: A Review. *Adv. Funct. Mater.* **2016**, *26*, 1678–1698. [[CrossRef](#)]
5. Wang, J.; Lu, C.; Zhang, K. Textile-Based Strain Sensor for Human Motion Detection. *Energy Environ. Mater.* **2020**, *3*, 80–100. [[CrossRef](#)]
6. Lakshmi, K.C.S.; Vedhanarayanan, B. High-Performance Supercapacitors: A Comprehensive Review on Paradigm Shift of Conventional Energy Storage Devices. *Batteries* **2023**, *9*, 202. [[CrossRef](#)]
7. Naoi, K.; Naoi, W.; Aoyagi, S.; Miyamoto, J.; Kamino, T. New Generation “Nanohybrid Supercapacitor”. *Acc. Chem. Res.* **2013**, *46*, 1075–1083. [[CrossRef](#)] [[PubMed](#)]
8. Yu, Z.; Tetard, L.; Zhai, L.; Thomas, J. Supercapacitor Electrode Materials: Nanostructures from 0 to 3 Dimensions. *Energy Environ. Sci.* **2015**, *8*, 702–730. [[CrossRef](#)]
9. Khan, Z.; Ail, U.; Ajjan, F.N.; Phopase, J.; Kim, N.; Kumar, D.; Khan, Z.U.; Nilsson, J.; Inganäs, O.; Berggren, M.; et al. Towards Printable Water-in-Polymer Salt Electrolytes for High Power Organic Batteries. *J. Power Sources* **2022**, *524*, 231103. [[CrossRef](#)]
10. Lakshmi, K.C.S.; Vedhanarayanan, B.; Cheng, H.Y.; Ji, X.; Shen, H.H.; Lin, T.W. Molecularly Engineered Organic Copolymers as High Capacity Cathode Materials for Aqueous Proton Battery Operating at Sub-Zero Temperatures. *J. Colloid Interface Sci.* **2022**, *619*, 123–131. [[CrossRef](#)]
11. Peng, K.; Zhang, J.; Yang, J.; Lin, L.; Gan, Q.; Yang, Z.; Chen, Y.; Feng, C. Green Conductive Hydrogel Electrolyte with Self-Healing Ability and Temperature Adaptability for Flexible Supercapacitors. *ACS Appl. Mater. Interfaces* **2022**, *14*, 39404–39419. [[CrossRef](#)] [[PubMed](#)]
12. Zhang, J.; Zhang, Q.; Liu, X.; Xia, S.; Gao, Y.; Gao, G. Flexible and Wearable Strain Sensors Based on Conductive Hydrogels. *J. Polym. Sci.* **2022**, *60*, 2663–2678. [[CrossRef](#)]
13. Chan, C.Y.; Wang, Z.; Jia, H.; Ng, P.F.; Chow, L.; Fei, B. Recent Advances of Hydrogel Electrolytes in Flexible Energy Storage Devices. *J. Mater. Chem. A* **2021**, *9*, 2043–2069. [[CrossRef](#)]
14. Amjadi, M.; Pichitpajongkit, A.; Lee, S.; Ryu, S.; Park, I. Highly Stretchable and Sensitive Strain Sensor Based on Silver Nanowire-Elastomer Nanocomposite. *ACS Nano* **2014**, *8*, 5154–5163. [[CrossRef](#)]
15. Liu, M.Y.; Hang, C.Z.; Wu, X.Y.; Zhu, L.Y.; Wen, X.H.; Wang, Y.; Zhao, X.F.; Lu, H.L. Investigation of Stretchable Strain Sensor Based on Cnt/AgNW Applied in Smart Wearable Devices. *Nanotechnology* **2022**, *33*, 255501. [[CrossRef](#)] [[PubMed](#)]
16. Ren, J.; Bai, W.; Guan, G.; Zhang, Y.; Peng, H. Flexible and Weaveable Capacitor Wire Based on a Carbon Nanocomposite Fiber. *Adv. Mater.* **2013**, *25*, 5965–5970. [[CrossRef](#)] [[PubMed](#)]
17. Chen, L.; Chang, X.; Wang, H.; Chen, J.; Zhu, Y. Stretchable and Transparent Multimodal Electronic-Skin Sensors in Detecting Strain, Temperature, and Humidity. *Nano Energy* **2022**, *96*, 107077. [[CrossRef](#)]
18. Chen, G.; Hu, O.; Lu, J.; Gu, J.; Chen, K.; Huang, J.; Hou, L.; Jiang, X. Highly Flexible and Adhesive Poly(Vinyl Alcohol)/Poly(Acrylic Amide-Co-2-Acrylamido-2-Methylpropane Sulfonic Acid)/Glycerin Hydrogel Electrolyte for Stretchable and Resumable Supercapacitor. *Chem. Eng. J.* **2021**, *425*, 131505. [[CrossRef](#)]
19. Yang, G.; Chen, J.; Liu, R.; Zhang, J.; Wang, R.; Chen, R.; Yang, H.; Fang, S. Sensing Applications of P(AAS-VPA)/P(EA-MAA) Composite Hydrogel with Highly Stretchability, Adhesion and Conductivity. *Polym. Mater. Sci. Eng.* **2022**, *38*, 156–166.
20. Sun, H.; Zhang, M.; Liu, M.; Yu, Y.; Xu, X.; Li, J. Fabrication of Double-Network Hydrogels with Universal Adhesion and Superior Extensibility and Cytocompatibility by One-Pot Method. *Biomacromolecules* **2020**, *21*, 4699–4708. [[CrossRef](#)]
21. Macarie, L.; Iliu, G. Poly(Vinylphosphonic Acid) and Its Derivatives. *Prog. Polym. Sci.* **2010**, *35*, 1078–1092. [[CrossRef](#)]

22. Bassi, A.K.; Gough, J.E.; Zakikhani, M.; Downes, S. The Chemical and Physical Properties of Poly(Epsilon-Caprolactone) Scaffolds Functionalised with Poly(Vinyl Phosphonic Acid-Co-Acrylic Acid). *J. Tissue Eng.* **2011**, *2011*, 615328. [[PubMed](#)]
23. Liu, R.; Milani, A.H.; Saunders, J.M.; Freemont, T.J.; Saunders, B.R. Tuning the Swelling and Mechanical Properties of Ph-Responsive Doubly Crosslinked Microgels Using Particle Composition. *Soft Matter* **2011**, *7*, 9297–9306. [[CrossRef](#)]
24. Zhao, L.; Ren, Z.; Liu, X.; Ling, Q.; Li, Z.; Gu, H. A Multifunctional, Self-Healing, Self-Adhesive, and Conductive Sodium Alginate/Poly(Vinyl Alcohol) Composite Hydrogel as a Flexible Strain Sensor. *ACS Appl. Mater. Interfaces* **2021**, *13*, 11344–11355. [[CrossRef](#)] [[PubMed](#)]
25. Pruneanu, S.; Boughriet, A.; Henderson, A.; Malins, C.; Ali, Z.; Olenic, L. Impedimetric Measurements for Monitoring Avidin-Biotin Interaction on Self-Assembled Monolayer. *Part. Sci. Technol.* **2008**, *26*, 136–144. [[CrossRef](#)]
26. Huang, X.; Guo, J.-Y.; Yang, J.; Xia, Y.; Zhang, Y.-F.; Fu, P.; Du, F.-P. High Mechanical Properties and Ionic Conductivity of Polysiloxane Sulfonate Via Tuning Ionization Degree with Clicking Chemical Reaction. *Polymer* **2022**, *254*, 125066. [[CrossRef](#)]
27. Li, L.; Zhao, J.; Zhao, H.; Qin, Y.; Zhu, X.; Wu, H.; Song, Z.; Ding, S. Structure, Composition and Electrochemical Performance Analysis of Fluorophosphates from Different Synthetic Methods: Is Really Na₃v₂(Po₄)₂f₃ Synthesized? *J. Mater. Chem. A* **2022**, *10*, 8877–8886. [[CrossRef](#)]
28. Wang, Q.; Zhang, Q.; Wang, G.; Wang, Y.; Ren, X.; Gao, G. Muscle-Inspired Anisotropic Hydrogel Strain Sensors. *ACS Appl. Mater. Interfaces* **2022**, *14*, 1921–1928. [[CrossRef](#)]
29. Zhang, Y.Z.; Lee, K.H.; Anjum, D.H.; Sougrat, R.; Jiang, Q.; Kim, H.; Alshareef, H.N. Mxenes Stretch Hydrogel Sensor Performance to New Limits. *Sci. Adv.* **2018**, *4*, eaat0098. [[CrossRef](#)]
30. Huang, H.; Han, L.; Fu, X.; Wang, Y.; Yang, Z.; Pan, L.; Xu, M. A Powder Self-Healable Hydrogel Electrolyte for Flexible Hybrid Supercapacitors with High Energy Density and Sustainability. *Small* **2021**, *17*, e2006807. [[CrossRef](#)]
31. Guo, Y.; Zheng, K.; Wan, P. A Flexible Stretchable Hydrogel Electrolyte for Healable All-in-One Configured Supercapacitors. *Small* **2018**, *14*, e1704497. [[CrossRef](#)] [[PubMed](#)]
32. Wang, K.; Zhang, X.; Li, C.; Sun, X.; Meng, Q.; Ma, Y.; Wei, Z. Chemically Crosslinked Hydrogel Film Leads to Integrated Flexible Supercapacitors with Superior Performance. *Adv. Mater.* **2015**, *27*, 7451–7457. [[CrossRef](#)] [[PubMed](#)]
33. Brezesinski, T.; Wang, J.; Tolbert, S.H.; Dunn, B. Ordered Mesoporous Alpha-Moo₃ with Iso-Oriented Nanocrystalline Walls for Thin-Film Pseudocapacitors. *Nat. Mater.* **2010**, *9*, 146–151. [[CrossRef](#)] [[PubMed](#)]
34. Li, K.; Wang, X.; Li, S.; Urbankowski, P.; Li, J.; Xu, Y.; Gogotsi, Y. An Ultrafast Conducting Polymer@Mxene Positive Electrode with High Volumetric Capacitance for Advanced Asymmetric Supercapacitors. *Small* **2020**, *16*, e1906851. [[CrossRef](#)]
35. Xia, X.; Chao, D.; Zhang, Y.; Zhan, J.; Zhong, Y.; Wang, X.; Wang, Y.; Shen, Z.X.; Tu, J.; Fan, H.J. Generic Synthesis of Carbon Nanotube Branches on Metal Oxide Arrays Exhibiting Stable High-Rate and Long-Cycle Sodium-Ion Storage. *Small* **2016**, *12*, 3048–3058. [[CrossRef](#)]
36. Choi, C.; Ashby, D.S.; Butts, D.M.; DeBlock, R.H.; Wei, Q.; Lau, J.; Dunn, B. Achieving High Energy Density and High Power Density with Pseudocapacitive Materials. *Nat. Rev. Mater.* **2019**, *5*, 5–19. [[CrossRef](#)]
37. Chen, Y.; Ren, H.; Rong, D.; Huang, Y.; He, S.; Rong, Q. Stretchable All-in-One Supercapacitor Enabled by Poly(Ethylene Glycol)-Based Hydrogel Electrolyte with Low-Temperature Tolerance. *Polymer* **2023**, *270*, 125796. [[CrossRef](#)]
38. Shan, C.; Che, M.; Cholewinski, A.; Ki Kunihiro, J.; Yim, E.K.F.; Su, R.; Zhao, B. Adhesive Hydrogels Tailored with Cellulose Nanofibers and Ferric Ions for Highly Sensitive Strain Sensors. *Chem. Eng. J.* **2022**, *450*, 138256. [[CrossRef](#)]
39. Bao, S.; Gao, J.; Xu, T.; Li, N.; Chen, W.; Lu, W. Anti-Freezing and Antibacterial Conductive Organohydrogel Co-Reinforced by 1d Silk Nanofibers and 2d Graphitic Carbon Nitride Nanosheets as Flexible Sensor. *Chem. Eng. J.* **2021**, *411*, 128470. [[CrossRef](#)]
40. Wang, L.; Gao, G.; Zhou, Y.; Xu, T.; Chen, J.; Wang, R.; Zhang, R.; Fu, J. Tough, Adhesive, Self-Healable, and Transparent Ionically Conductive Zwitterionic Nanocomposite Hydrogels as Skin Strain Sensors. *ACS Appl. Mater. Interfaces* **2019**, *11*, 3506–3515. [[CrossRef](#)]
41. Zhang, Q.; Liu, X.; Ren, X.; Jia, F.; Duan, L.; Gao, G. Nucleotide-Regulated Tough and Rapidly Self-Recoverable Hydrogels for Highly Sensitive and Durable Pressure and Strain Sensors. *Chem. Mater.* **2019**, *31*, 5881–5889. [[CrossRef](#)]
42. Hu, C.; Zhang, Y.; Wang, X.; Xing, L.; Shi, L.; Ran, R. Stable, Strain-Sensitive Conductive Hydrogel with Antifreezing Capability, Remoldability, and Reusability. *ACS Appl. Mater. Interfaces* **2018**, *10*, 44000–44010. [[CrossRef](#)]
43. Li, S.; Pan, H.; Wang, Y.; Sun, J. Polyelectrolyte Complex-Based Self-Healing, Fatigue-Resistant and Anti-Freezing Hydrogels as Highly Sensitive Ionic Skins. *J. Mater. Chem. A* **2020**, *8*, 3667–3675. [[CrossRef](#)]
44. Ge, G.; Yuan, W.; Zhao, W.; Lu, Y.; Zhang, Y.; Wang, W.; Chen, P.; Huang, W.; Si, W.; Dong, X. Highly Stretchable and Autonomously Healable Epidermal Sensor Based on Multi-Functional Hydrogel Frameworks. *J. Mater. Chem. A* **2019**, *7*, 5949–5956. [[CrossRef](#)]
45. Ren, J.; Liu, Y.; Wang, Z.; Chen, S.; Ma, Y.; Wei, H.; Lü, S. An Anti-Swellable Hydrogel Strain Sensor for Underwater Motion Detection. *Adv. Funct. Mater.* **2021**, *32*, 2107404. [[CrossRef](#)]
46. Liu, X.; Qin, J.; Wang, J.; Chen, Y.; Miao, G.; Zheng, J.; Liu, X. Preparation and Properties of Cellulose Nanofibers/A-Zirconium Phosphate Nanosheets Composite Polyvinyl Alcohol Ion-Conductive Organohydrogel and Its Application in Strain Sensors. *J. Appl. Polym. Sci.* **2022**, *139*, e53076. [[CrossRef](#)]

Disclaimer/Publisher's Note: The statements, opinions and data contained in all publications are solely those of the individual author(s) and contributor(s) and not of MDPI and/or the editor(s). MDPI and/or the editor(s) disclaim responsibility for any injury to people or property resulting from any ideas, methods, instructions or products referred to in the content.